Active Control of Variable DC-Link for Maximum Efficiency of Traction Motor Drives

Active Control of Variable DC-link for Maximum Efficiency of Traction Motor Drives

Paolo Pescetto, *Member, IEEE,* Andres Sierra-Gonzalez, *Student Member, IEEE,* Fernando Alvarez-Gonzalez, Hansjörg Kapeller, Elena Trancho, *Member, IEEE,* Gianmario Pellegrino, *Fellow, IEEE*

***Abstract*—Modern electric vehicles often interpose a DC/DC converter between traction battery and inverter, boosting the supply voltage of the drive. The power losses in the two converters and in the electric motor significantly vary with the DC-link voltage amplitude. In this work, a novel control algorithm is proposed to adapt online the DC-link voltage during vehicle operation, pursuing the maximum efficiency of the DC/DC converter and traction inverter without affecting the motor control dynamic. The key principle of the proposal, suitable for 3-phase and multi-three-phase drives, relies on the DC-link voltage minimization on varying the drive operating conditions. Among its advantages, the proposed variable DC-link control is independent of the motor parameters, the adopted torque/speed control strategy and the number of 3-phase sets of the drive. Although originally developed for electric vehicles, it can be adopted in a wide number of applications. Straightforward calibration roles are also provided. The proposed algorithm is deeply validated in simulation and experiments using a full-scale 135 kW 6-phase traction motor drive at TRL6.**

***Index Terms*—Electric vehicles, Variable DC-link, Motor drives, DC/DC converter, Efficiency improvement, Loss minimization, Multiphase machines.**

I. Introduction

In the last decade, the trade of Battery Electric Vehicles (BEVs) rapidly grew [1] because of several factors, including their lower environmental and acoustic impact with respect to traditional combustion engines, their decreasing price, and, in several countries, favorable legislation. The rapid spread of BEVs leads to increasing expectations from the users, translated into stricter requirements for the electric components. A major Key Performance Indicator (KPI) of a BEV is its efficiency, normally evaluated over standard driving cycles, such as Worldwide Harmonized Light Vehicles Test Procedure (WLTP). The power loss in the e-axle significantly affects the cooling requirements, rated power, overload capability [2], and compactness. In this scenario, multi-three-phase drives, already widely present in high power applications such as wind turbines, ship propulsion, and aerospace [3], [4], are becoming appealing also for automotive, permitting higher power ratings with reduced phase currents, higher reliability, and benefits in thermal management [5]. In particular, the 6-phase solution, or dual-three-phase, was recently explored by several projects [6]–[8], as it offers a good trade-off between improved motor performance and increased drive complexity.

The traction battery is among the most sensitive components of a BEV. A high battery voltage v_b permits increasing the motor control dynamic and drive compactness with a lower phase current, with possibly higher motor efficiency, whereas low voltage batteries are easier to be manufactured in compliance with the safety requirements. To solve this trade-off, several EVs [7], [9], including the one under test reported in Fig. 1, interpose a bidirectional DC/DC converter between the battery and the traction inverter, permitting boost the drive voltage rating despite a reduced v_b. The main downside of this solution is that the DC/DC converter introduces additional losses during driving, affecting the BEV efficiency. To mitigate this drawback, the DC-link voltage can be online adapted on varying the drive operating point [10], pursuing minimum losses of the converters and motor [11], [12]. Nevertheless, most of the available variable v_{dc} techniques [10], [13]–[18] require a fast dynamic control of the DC-link, that is feasible only if the DC/DC and the inverter are integrated into the same converter and the respective controls are executed by the same control board with negligible delay. Moreover, techniques like [10], [13]–[17] require the motor control being custom designed together with the DC/DC control. A further constraint is given to the size of the DC-link capacitors to allow a fast v_{dc} variation. Additionally, methods such as [13], [16], [17] exploit non-standard DC/DC converters, which may not be accepted for large scale production. Finally, none of the above-cited control strategies is suitable for multiphase drives.

This work proposes a novel algorithm to minimize the losses in the DC/DC converter and in the traction inverter by effectively adapting v_{dc} without reducing the motor control dynamic. The switching losses in the two converters are reduced by minimizing the DC-link voltage, still guaranteeing

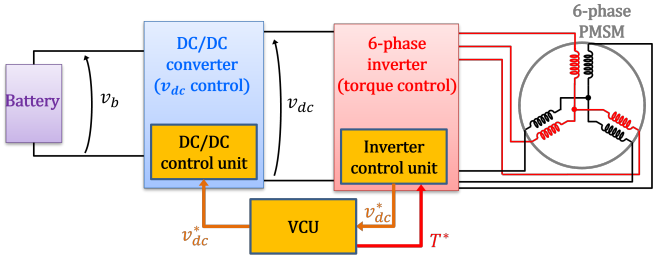

Fig. 1. Considered EV powertrain [6], [7].

Paolo Pescetto (*paolo.pescetto@polito.it*) and Gianmario Pellegrino (*gianmario.pellegrino@polito.it*) are with the Energy Department *Galileo Ferraris*, Politecnico di Torino, Torino, Italy.

Andres Sierra-Gonzalez (*andres.sierra@tecnalia.com*), Fernando Alvarez-Gonzalez (*fernando.alvarez@tecnalia.com*), and Elena Trancho (*elena.trancho@tecnalia.com*) are with TECNALIA, Basque Research and Technology Alliance (BRTA), Bilbao, Spain.

Hansjörg Kapeller (*Hansjoerg.Kapeller@ait.ac.at*) is with AIT Austrian Institute of Technology, Vienna, Austria.

optimal motor control. Among its benefits, the proposed variable DC-link control is independent of the motor control strategy and calibration, so the motor and DC/DC controls can be developed, debugged, and calibrated separately, with large freedom for the designers. The proposed variable v_{dc} control is also independent of the ratings or type of the electric machine, being either a synchronous or an induction motor. Moreover, the algorithm is also applicable for multi-three-phase drives, regardless of the number of 3-phase sets. Finally, the proposed method is robust against execution delay of the DC/DC converter, so it can be implemented independently on the DC/DC being integrated or not with the traction inverter and whatever its internal structure. In turn, despite the proposed adaptive DC-link control was designed for a specific EV architecture, it can be applied to a wide number of applications adopting a controlled DC-link. Since it is developed independently by the motor control, the proposal is a feasible add-on to existing drive applications. This paper follows its conference version [19] with substantial improvements, including:

- possible benefits of the proposed technique on the motor operation are discussed, including reduction of copper and iron PWM loss for low-inductance motors;
- a full calibration procedure is given, permitting a fast implementation of the proposed technique;
- if [19] was supported by simulation results only, a comprehensive experimental validation is now included on a full scale 135 kW traction drive at high Technology Readiness Level (TRL6) [20];
- the energy saving obtained by the present technique has been evaluated over a WLTP homologation driving cycle.

II. Vehicle Architecture

The architecture and ratings of the A-segment BEV under test [7] are reported in Fig. 1 and Table I. Depending on the State Of Charge (SOC), the battery voltage v_b varies between 320 V and 420 V with a rated value of 370 V. A bidirectional automotive grade DC/DC boost converter [21] elevates v_b to a regulated DC-link with a maximum v_{dc} of 750 V:

$$1.1 \cdot v_b < v_{dc} < 750V \tag{1}$$

The boosted DC-link supplies the 6-phase inverter, feeding the traction motor. The inverter implements the motor torque control, actuating the reference torque T^* set by the driver. Meanwhile, the DC/DC regulates the v_{dc}, aiming to minimize the power loss in the two converters. The two converters are physically separated, without a direct communication between them. The proposed variable v_{dc} algorithm, executed in the Inverter Control Unit (ICU), computes the reference v_{dc}^*, which is communicated via CAN protocol to the Vehicle Control Unit (VCU) and ultimately to the DC/DC control unit, with a delay of 20 to 22 ms between the v_{dc}^* determination in the ICU and its execution. On top of this, the DC/DC presents an internal voltage control bandwidth of 160 Hz, producing an additional delay of 3 ms, leading to a total execution delay of ≈25 ms, which is highly relevant if compared with the motor control dynamic and dominates the bandwidth of the v_{dc} control. Therefore, in this vehicle architecture, the methods like [10], [13]–[16] could not be implemented, as they require a sufficiently high v_{dc} control bandwidth to adapt the DC-link on varying the rotor position.

TABLE I
E-Axle Ratings.

DC/DC converter		**e-Drive**	
Battery voltage (V)	320÷420*	Number of phases	3/6
Max v_{dc} (V)	750	PWM frequency (kHz)	12
Cont. power (kW)	180	Cont. torque (Nm)	80
		Peak torque (Nm)	170
		Peak power (kW)	135
		Max speed (krpm)	22
		Max current (Arms)	235

The motor is a Permanent Magnet Synchronous Machine (PMSM) designed for high efficiency and torque density, despite the non-linear magnetic saturation characteristic [22]. It presents two symmetrical 3-phase winding sets, i.e., the two sets present a phase shift of 60°, with high magnetic coupling. The two sets can be reconfigured in 3-phase or 6-phase mode for development and testing purposes. In 3-phase mode, the two sets are connected in parallel to double the phase current capability maintaining the same rated voltage.

III. BEV Loss Analysis

A. Efficiency Maps of the Converters

In a PWM inverter, the DC-link voltage marginally affects the conduction losses, while the switching losses grow almost linearly with v_{dc} [23], reducing the inverter efficiency. For the adopted inverter, the loss variation with v_{dc} is given in Fig. 2a at different phase currents, corresponding to different motor torque. This loss map was initially derived from Spice simulations of the power semiconductors manufacturer and then refined based on experimental measurements [6]. The inverter efficiency reduction with increasing v_{dc} is clearly visible.

Similarly, a lower v_{dc} reduces the switching losses in the DC/DC converter, but for equal power demand, the output current increases, thus increasing the conduction losses. Determining the optimal v_{dc} minimizing the DC/DC losses may not be trivial, and it depends on the power modules technology and the ratio between switching and conduction losses. Anyway, the switching loss reduction is commonly predominant. The efficiency of the commercial DC/DC under test [21] on varying the operating point was experimentally measured [6] in cooperation with the converter's manufacturer, leading to the loss maps reported in Fig. 2b. The reported losses aggregate the conduction and switching losses in the power electronic components, the losses in the reactive elements, and in the control circuitry. It is confirmed that efficiency improves at lower v_{dc} at any level of battery current and voltage.

B. PWM Loss in the Electric Motor

The electromagnetic power loss in an electric motor can be classified into copper (or Joule) and iron losses. With respect to a sinusoidal excitation, an inverter fed electric motor presents

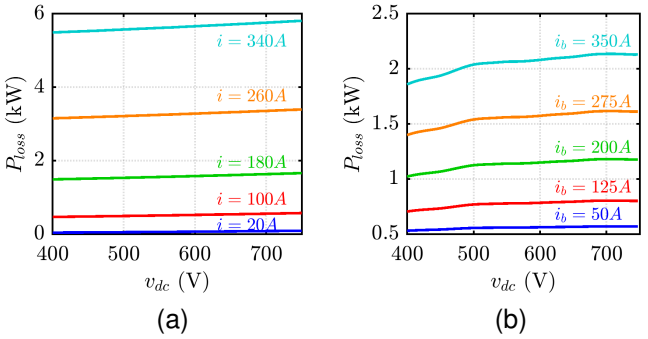

Fig. 2. Power losses on varying v_{dc} (a) in the 6-phase inverter at different phase currents and (b) in the DC/DC converter at different battery currents

additional power loss due to the PWM excitation [12], [24], [25], causing a ripple in the phase current that increases its RMS value and the related Joule loss. In high speed traction PMSMs, this effect can be particularly significant due to the low machine inductance, producing a high PWM current ripple. Moreover, the iron losses are increased because of the bipolar voltage excitation within the PWM period, producing additional eddy currents and minor hysteresis loops.

The additional PWM losses in both the copper and iron depend on the DC-link amplitude [12]. A lower v_{dc} produces lower current ripple and lower voltage excitation at PWM frequency, decreasing the related additional Joule and iron losses. For the same operating point of the machine in the dq plane, the additional Joule loss and eddy current loss are approximately proportional to v_{dc}^2, while the loss due to minor hysteresis loops grows nonlinearly with v_{dc}. Therefore, a control strategy minimizing the DC-link voltage is also beneficial to reduce the additional PWM loss. On the other side, a low v_{dc} reduces the base speed (2), anticipating the necessity of field weakening and resulting in higher current and fundamental losses at medium and high speed. This is avoided by the proposed strategy (see Section V).

IV. Motor Torque Control

This work proposes a variable DC-link control independent of the motor control algorithm and the number of 3-phase sets of the drive. To prove this aspect, the proposal was tested combined with different motor control strategies: a 3-phase Current Vector Control-Field Oriented Control (CVC-FOC) [28], a 3-phase Direct Flux Vector Control (DFVC) [27], and a 6-phase CVC-FOC [26]. Both DFVC and CVC-FOC operate on the MTPA below the base speed ω_b, while FW is necessary at higher speed to meet the maximum voltage constraint, despite the lower drive efficiency:

$$\omega_b \approx \frac{\frac{v_{dc}}{\sqrt{3}} - R_s|\boldsymbol{i_{dq}}|}{\lambda}, \tag{2}$$

where $\boldsymbol{i_{dq}}$ is the current vector, $\lambda = |\boldsymbol{\lambda_{dq}}|$ is the amplitude of the stator flux vector and R_s is the stator resistance. Since the base speed increases with v_{dc}, the MTPA speed range can be extended by properly adapting v_{dc} (and so ω_b), thus reducing the motor Joule losses. Since this is not the focus

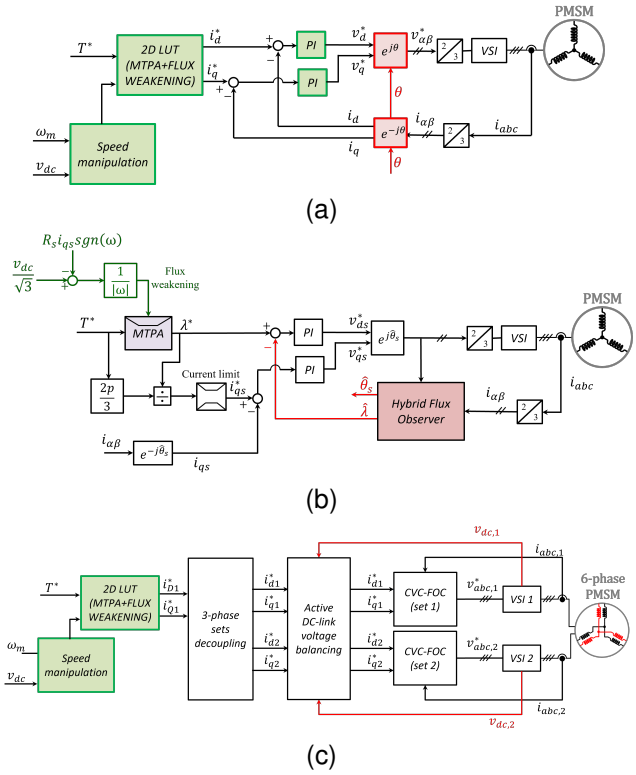

Fig. 3. Tested torque control algorithms. (a) 3-phase CVC-FOC; (b) 3-phase DFVC; (c) 6-phase CVC-FOC.

of the paper, the tested torque control strategies are only synthetically described here.

In all the considered torque controls, a maximum efficiency strategy considering copper and iron motor loss could be adopted in place of the MTPA locus to pursue deeper loss minimization. This would be doable by replacing the MTPA LUTs with maximum efficiency LUTs. Anyway, the proposed variable v_{dc} control strategy would not be affected, as it is independent of the motor control algorithm.

A. 3-phase CVC-FOC

The CVC-FOC [28] consists of two current control loops, regulating the state variables i_d and i_q, with the reference vector $\boldsymbol{i_{dq}^*}$ determined by means of Look-Up Tables (LUTs). $\boldsymbol{i_{dq}^*}$ is forced on the MTPA if the speed is below $\omega_b(v_{dc})$ and moved to the field weakening region otherwise. The optimal current reference depends on the torque request T^*, the motor speed n, and v_{dc}, thus requiring LUTs in three dimensions (3D LUTs). In this implementation [28], depicted in Fig. 3a, the LUTs dimension is reduced to two thanks to a speed manipulation, which considers the v_{dc} variability. This permits a reliable torque control under relevant DC-link variations with lower complexity of the LUTs (2D LUTs).

B. 3-phase DFVC

The DFVC scheme [27], depicted in Fig. 3b, operates in stator flux coordinates (d_s, q_s), closed loop imposing the flux amplitude λ and its quadrature current i_{qs}. A hybrid flux observer merges the flux estimation based on the current

model, i.e., the flux maps and the back-EMF integration. The reference flux amplitude λ^* is set based on MTPA locus, and flux weakening is obtained by limiting λ^* based on the electrical speed ω and v_{dc}, permitting accurate torque control under variable v_{dc} both on MTPA and flux weakening.

C. 6-phase CVC-FOC

The 6-phase CVC-FOC in [26] was adopted, depicted in Fig. 3c. The current set-point generation is similar to the 3-phase case, with two current vector controls for the two 3-phase sets. An additional block is required to decouple the two 3-phase sets. Moreover, the adopted traction drive [7] presents a cascade connection of the two 3-phase inverters (see Fig. 6.b), requiring a dedicated control for balancing the two halves of the DC-link.

V. Proposed Variable DC-link Control

The variable v_{dc} control was initially developed for an equivalent 3-phase drive and then extended to the 6-phase case. The adopted criteria are:

1) inverter and DC/DC efficiencies improve at lower v_{dc}
2) the MTPA speed region must be maximized
3) the motor control dynamic must not be deteriorated
4) for standard 3-phase modulation, the maximum amplitude of the voltage vector that can be synthesized is

$$|\boldsymbol{v^*_{\alpha\beta}}|_{max} = v_{dc}/\sqrt{3} \tag{3}$$

A. DC-link Control for a 3-phase Drive

The variable DC-link control is reported in Fig. 4, where v_{dc} is minimized to reduce the converters' switching loss while permitting the correct operation of the motor control. Whatever the adopted algorithm, the motor control outputs the reference voltage vector in stationary frame $\boldsymbol{v^*_{\alpha\beta}}$, which is adopted to compute the signal v_o^*:

$$v_o^* = \sqrt{3} \cdot k_{DCDC} |\boldsymbol{v^*_{\alpha\beta}}| \tag{4}$$

where $k_{DCDC} > 1$ is a scalar gain. According to (3), a DC-link voltage equal to v_o^* guarantees that the reference $\boldsymbol{v^*_{\alpha\beta}}$ can be synthesized by the inverter, and the k_{DCDC} gain defines the voltage safety margin. A high k_{DCDC} permits higher voltage margin, and so a more reliable motor control, but it also leads to a higher v_{dc}, thus increasing the switching losses. To meet this trade-off, k_{DCDC} is online adapted based on the

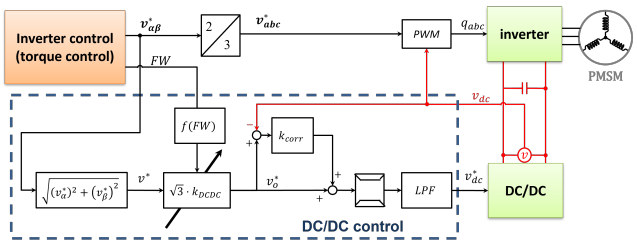

Fig. 4. Block diagram of the proposed DC-link control for a 3-phase drive.

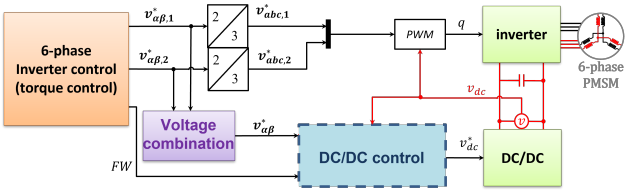

Fig. 5. Block diagram of the DC-link control extended to a 6-phase drive.

FW signal, which is a flag indicating if the motor control is operating on the MTPA ($FW = 0$) or in field weakening region ($FW = 1$), where the required $\boldsymbol{v^*_{\alpha\beta}}$ is close to the maximum voltage limit. More details on k_{DCDC} adaptation are given in Section VI-A. Then, the difference between v_o^* and the measured v_{dc} is multiplied by the correction gain k_{corr} and added to v_o^*. The obtained signal, saturated based on the DC/DC converter operating limits in (1), is Low-Pass Filtered (LPF) to get the reference v_{dc}^*.

$$v_{dc}^* = LPF(v_o^* + k_{corr}\,(v_o^* - v_{dc})) \tag{5}$$

At steady state, $v_{dc} = v_o^*$ and so this correction branch is ineffective, permitting the system operation at minimum v_{dc}. Conversely, during sharp transients, $v_{dc} \neq v_o^*$ due to the serious actuation delay in the DC/DC converter (see Section II), and the correction branch boosts the DC/DC control dynamic. This permits fulfilling the criterion 3). Finally, v_{dc}^* is communicated to the DC/DC converter and executed, as said, with a significant delay of ≈25 ms.

It should be noted that according to criterion 2), the MTPA speed range is extended as far as possible. For a given torque, if the speed increases (and so the motor voltage), the DC/DC control progressively boosts v_{dc}, permitting MTPA operation. Field weakening is only actuated when v_{dc} is saturated to the maximum operating limit of the DC/DC converter, thus minimizing the motor Joule loss. Overall, the drive efficiency is increased in the full torque and speed operating domain, automatically imposing the lowest v_{dc} which permits avoiding or limiting the field weakening, contemporary achieving high efficiency at low speed and high dynamic at high speed.

B. Extension to 6-phase Drive

After being tested in 3-phase motors, the proposed adaptive DC-link control was extended to the dual-three-phase case, with the control block scheme reported in Fig. 5. The variable v_{dc} control strategy, calibration, and dynamic are not changed, but the input voltage $\boldsymbol{v^*_{\alpha\beta}}$ is a combination of the reference voltages of the two 3-phase sets $\boldsymbol{v^*_{\alpha\beta,1}}$ and $\boldsymbol{v^*_{\alpha\beta,2}}$.

The combination law of $\boldsymbol{v^*_{\alpha\beta,1}}$ and $\boldsymbol{v^*_{\alpha\beta,2}}$ depends on the 6-phase drive topology. The most common topology is depicted in Fig. 6.a, with the DC inputs of the two 3-phase inverter units parallel connected. Here, the input of the DC/DC control will be the voltage vector having a larger amplitude:

$$|\boldsymbol{v^*_{\alpha\beta}}| = max\left(|\boldsymbol{v^*_{\alpha\beta,1}}|, |\boldsymbol{v^*_{\alpha\beta,2}}|\right) \tag{6}$$

This guarantees sufficient v_{dc} to control both the 3-phase sets without affecting the torque control dynamic.

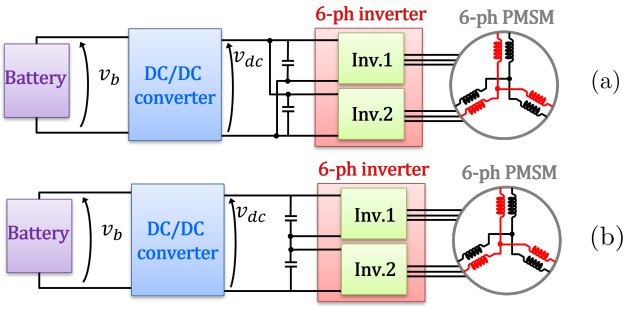

Fig. 6. Possible connection of dual-three-phase inverters. (a) Parallel connection. (b) Cascade connection.

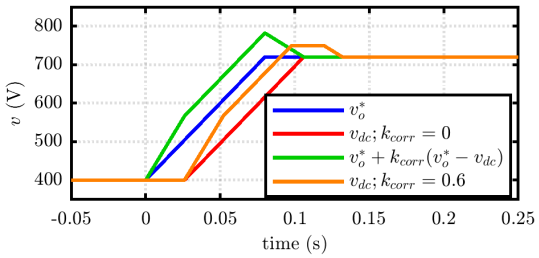

Fig. 7. k_{corr} calibration. Blue: sharp ramp of v_o^*; red: resulting v_{dc} in absence of compensation branch; orange: v_{dc} with the compensation branch.

Another feasible solution is to connect the 3-phase inverter units in cascade, as in Fig. 6.b. This is the topology adopted in the 6-phase drive under test [7]. In this case, the DC/DC controls the total DC-link voltage, while each inverter is fed by half of v_{dc}. The torque control must include a voltage balancing algorithm, as in Fig. 3c, to ensure the DC-link is equally split between the two inverters [26]. The adopted combination law of the two reference voltage vectors is:

$$|\boldsymbol{v}^*_{\boldsymbol{\alpha\beta}}| = |\boldsymbol{v}^*_{\boldsymbol{\alpha\beta,1}}| + |\boldsymbol{v}^*_{\boldsymbol{\alpha\beta,2}}| \tag{7}$$

Overall, for any multiphase converters topologies, a proper combination law can be easily found, even with a number of three-phase sets higher than 2, confirming the wide applicability of the proposed variable DC-link control regardless of the drive number of phases.

VI. Control Calibration

The proposed control only presents a few parameters to be tuned. This Section provides a calibration guideline, valid both for 3-phase and multi-three-phase drives.

A. Adaptation of k_{DCDC} Gain

At steady state, the DC-link voltage results:

$$v_{dc} = \sqrt{3}|\boldsymbol{v}^*_{\boldsymbol{\alpha\beta}}| \cdot k_{DCDC} \tag{8}$$

So, the scalar gain k_{DCDC} defines the DC-link voltage margin. As an example, setting k_{DCDC}=1.1 guarantees 10% voltage margin. The calibration of k_{DCDC} is a trade-off between control performance and optimal voltage utilization. A high k_{DCDC} provides a larger voltage margin, enhancing the torque control stability under sharp speed or torque transients. Conversely, a low k_{DCDC} effectively minimizes v_{dc}, thus reducing the switching losses in the two converters, which are particularly significant at steady-state. This trade-off is solved by linearly varying k_{DCDC} between a minimum k^{min}_{DCDC} and a maximum k^{max}_{DCDC}. In particular, k_{DCDC} is bounded between a minimum k^{min}_{DCDC} and a maximum k^{max}_{DCDC} value, and it is ramped up for $FW = 1$ and it is ramped down for $FW = 0$.

At steady-state, if the drive operates on MTPA, the FW signal is null and k_{DCDC} converges to k^{min}_{DCDC}, permitting to minimize the switching losses, while if the motor works in field weakening, v_{dc} is anyway saturated to the maximum value, regardless k_{DCDC}. During a sharp torque or speed transient, $|\boldsymbol{v}^*_{\boldsymbol{\alpha\beta}}|$ may suddenly increase, requiring a higher v_{dc}, while the DC/DC control dynamic is limited by its actuation delay. If $|\boldsymbol{v}^*_{\boldsymbol{\alpha\beta}}|$ overcomes the voltage limit, the drive tends to operate in field weakening, leading to $FW = 1$. As a result, k_{DCDC} is linearly raised to k^{max}_{DCDC}, permitting larger voltage margin and stable motor control during sharp transients. In turn, the voltage margin is defined by k^{min}_{DCDC} under MTPA steady state and by k^{max}_{DCDC} during a transient.

In the considered drive, as for most of the applications, due to hardware constraints, the full DC-link cannot be exploited, as the inverter duty cycles are bounded in the range $[d_{min}\ d_{max}]$. This limitation permits calibrating k^{min}_{DCDC} as:

$$k^{min}_{DCDC} \geq \frac{1}{d_{max} - d_{min}} \tag{9}$$

In this implementation, the duty cycles are limited within [0.03 0.97], leading to k^{min}_{DCDC}=1.1. About k^{max}_{DCDC}, the maximum slew-rate of voltage variation must be considered. The worst case scenario is a sharp motor acceleration under the maximum torque, causing a voltage slew rate of:

$$max\left(\frac{dv^*}{dt}\right) \approx \dot{\omega}_{max} \cdot \lambda\left(T_{max}\right) \tag{10}$$

where $\dot{\omega}_{max}$ is the maximum electrical acceleration, defined by the application, and $\lambda\left(T_{max}\right)$ is the stator flux amplitude at maximum torque. Considering the actuation delay t_d, accounting for the communication delay and the LPF effect, the gain k^{max}_{DCDC} can be calibrated as:

$$k^{max}_{DCDC} \geq \left(1 + \frac{\sqrt{3}\dot{\omega}_{max}\lambda t_d}{v_{dc}}\right) \cdot \frac{1}{d_{max} - d_{min}} \tag{11}$$

In this implementation k^{max}_{DCDC} was set at 1.2.

B. Correction Gain

The correction branch is ineffective when $v_{dc} = v_o^*$, i.e., at steady state, while it boosts the $v_{dc}*$ reference dynamic during transients. This partially compensates for the relevant DC/DC actuation delay described in Section II.

The correction gain k_{corr} defines the amplitude of the feed-forward term in Fig. 4. A typical test case is depicted in Fig. 7, reporting a sharp ramp of voltage request v_o^* from 400 V to 720 V (blue line), where the effect of the LPF has been

neglected. In the absence of correction branch (i.e., $k_{corr} = 0$), the obtained v_{dc} is lagging by 25 ms due to the actuation delay. If the correction branch is included, the green line represents the voltage signal after the feed-forward term $k_{corr}\,(v_o^* - v_{dc})$. The resulting v_{dc} (orange line) is again delayed by 25 ms and saturated between the operating limits of the DC/DC converter. As can be noted, the actuation delay is largely compensated during the voltage ramp at the cost of a slight overshoot. Based on this approach, a perfect compensation is obtained for $k_{corr} = 1$, but this can lead to a relatively large overshoot at the end of the voltage ramp. If $k_{corr} < 1$ is set, the overshoot is limited, still partially compensating the actuation delay. In this work, k_{corr} was set to 0.6.

C. Low-Pass Filter

The LPF, although limiting the bandwidth of the v_{dc} control, avoids possible interactions between motor control and variable DC-link control, which may lead to an underdamped response. The motor control normally has a bandwidth of several hundreds of Hz, i.e., much faster than the v_{dc} control, so the response time of the torque control is neglected for LPF calibration. In absence of LPF, the response time of the variable v_{dc} control would be equal to the actuation delay, which in our case is 25 ms. Therefore, the interaction between the variable DC-link control and the motor torque control would produce an oscillation in v_{dc} having a period of 25 ms, corresponding to a frequency of 40 Hz. These oscillations are damped by the LPF, provided that it is calibrated sufficiently slower. In this implementation, the LPF cut-off frequency was set at 30 Hz. A higher bandwidth is feasible at the cost of relevant oscillations in the v_{dc} response. This is acceptable only if the torque control is sufficiently robust under fast DC-link variations. More details are given in Section VII.

VII. Simulation Results

The proposed adaptive DC-link control was validated in MATLAB-Simulink environment when combined with different torque control strategies while the motor speed is externally imposed. The simulations are performed to demonstrate the stability and robustness of the proposed technique under severe speed and load transients. With this goal, the maximum torque and speed slew rates were set considerably higher than the actual ratings in the BEV (acceleration at +15000 rpm/s, corresponding to 135 (km/h)/s, braking at -30000 rpm/s, i.e., -270 (km/h)/s, torque slew rate of 1500 Nm/s). The achieved advantages in terms of loss reduction are demanded to the experimental session, reported in Section VIII. Table I reports the system's ratings.

At first, in Fig. 8, the motor has been controlled in DFVC in 3-phase configuration [27] (see Fig. 3b) at rated torque reference T^*=80 Nm, to verify the steady-state stability at 2000 rpm, 4500 rpm, and 8000 rpm. The upper subplot depicts the torque and speed, the middle subplot shows the flux and current amplitude, and the maximum flux limit λ_{max} (black line) computed as in [27]. The DFVC operates on the MTPA when $\lambda < \lambda_{max}$, whereas it imposes field weakening when $\lambda = \lambda_{max}$. The third subplot depicts the controlled DC-link voltage and the amplitude of the vector $\boldsymbol{v}^*_{\boldsymbol{\alpha\beta}}$ multiplied by $\sqrt{3}$, i.e., the minimum DC-link voltage required to synthesize the reference $\boldsymbol{v}^*_{\boldsymbol{\alpha\beta}}$, as per (3). Fig. 8 highlights three regions of operation. At low speed, i.e., for t <1.5 s, the minimum DC-link voltage suffices for controlling the machine on the MTPA, so the command v^*_{dc} is saturated at its minimum value (400 V). At medium speed (4500 rpm, 1.5 s< t <2.5 s), the minimum v_{dc} is not sufficient for MTPA operation, and the motor control tends to work in flux weakening. This is avoided by increasing the DC-link to 580 V, slightly higher than $\sqrt{3}|\boldsymbol{v}^*_{\boldsymbol{\alpha\beta}}|$. It should be noted that the current and flux amplitude at 4500 rpm and 2000 rpm are equal, confirming that the drive is still operating on MTPA. At 8000 rpm or higher (t >2.5 s), the v^*_{dc} is saturated to its maximum operating limit (750 V), the MTPA cannot be tracked and flux weakening is physically unavoidable, resulting in a lower $|\lambda|$ and a higher current. Since the drive works at the maximum v_{dc}, the operating point is as close as possible to the MTPA locus.

In the test reported in Fig. 9, the drive is still controlled in 3-phase DFVC but under a complex operating cycle. The simulation starts at zero torque and speed. Then, a step of T^* =100 Nm (25% overload) is demanded. Being at standstill, the corresponding $|\boldsymbol{v}^*_{\boldsymbol{\alpha\beta}}|$ is low and the variable DC-link control converges at the minimum v_{dc}, sufficient for MTPA operation. At t=0.5 s, the motor is sharply accelerated to 7500 rpm, i.e., 20% over the base speed. As soon as the voltage reference gets close to saturation, the variable DC-link control correctly reacts by progressively increasing v_{dc} up to the maximum value (750 V), moving then to unavoidable field weakening. At t=1.5 s, the torque is reversed to -100 Nm. As the torque transiently passes through zero, the required voltage is also transiently reduced; the maximum v_{dc} is unnecessary and the variable DC-link control reduces v^*_{dc}. This results in a small drop in v_{dc}, promptly recovered as the negative torque increases. The speed is reversed to -7500 rpm at t=2 s; v_{dc} is correctly reduced when the speed decreases, thus requiring lower voltage, and again increased when the speed increases in negative direction. In turn, the motor control is stable even under severe transients and/or flux weakening conditions, while the adaptive DC-link control properly imposes the minimum v_{dc}, limiting the flux weakening.

The same load cycle is reported in Fig. 10, but with the drive in 6-phase configuration under CVC-FOC [26]. Also,

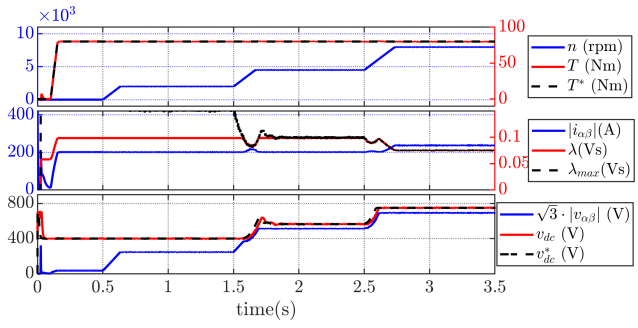

Fig. 8. Simulation of DC/DC control combined with 3-phase CVC-FOC: steady state operation at 2000, 4500, and 8000 rpm, rated torque.

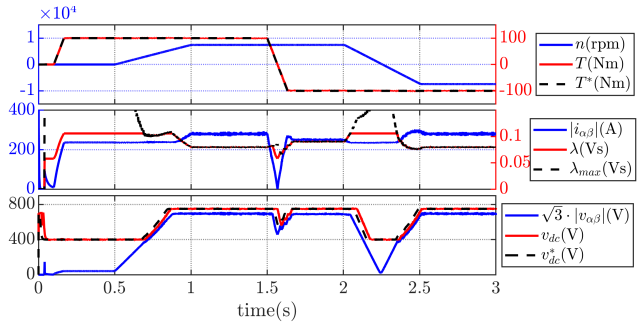

Fig. 9. Simulation of DC/DC control combined with DFVC torque control for 3-phase configuration: complex load cycle.

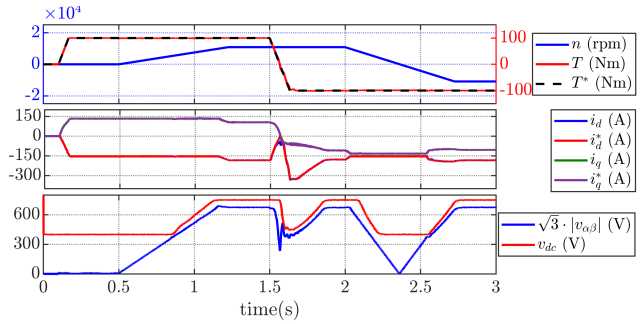

Fig. 10. Simulation of DC/DC control combined with CVC-FOC torque control for 6-phase configuration: complex load cycle.

in this case, the control works properly, with the reference torque accurately tracked and v_{dc} correctly imposed at its minimum. The main difference compared to the DFVC case is a larger voltage sag under torque reversal, which is explained considering the inherently higher capability of the DFVC of accurate and fast torque regulation under flux weakening respect to the CVC-FOC. In both cases, the motor torque control dynamic is not limited by the variable DC-link control, so the torque can be regulated at the best capabilities of the motor control algorithm.

Finally, Figs. 11 and 12 highlight the influence of LPF cut-off frequency on the control stability for 3-phase DFVC. In both tests, a sharp torque reversal from +100 Nm to -100 Nm is commanded at 7500 rpm, with the LPF cut-off frequency set at 30 Hz and 150 Hz, respectively. As can be noted, the 30 Hz LPF can properly avoid the interactions between motor control and variable DC-link control, as v_{dc} is stable and smooth. On the other hand, the test with the LPF at 150 Hz presents a significant DC-link oscillation with a frequency of 25 ms, as expected from Section VI-C, These oscillations do not affect the torque control thanks to the inherent torque accuracy of the DFVC under variable DC-link, but it may be critical in other types of control, such as CVC.

VIII. Experimental Results

The adopted setup is reported in Fig. 13. The proposed technique was tested on a full-scale traction drive [6] at high Technology Readiness Level (TRL6) [20]. The demonstration at such a high TRL effectively proves the rapid applicability of the proposal in the target application. The architecture depicted

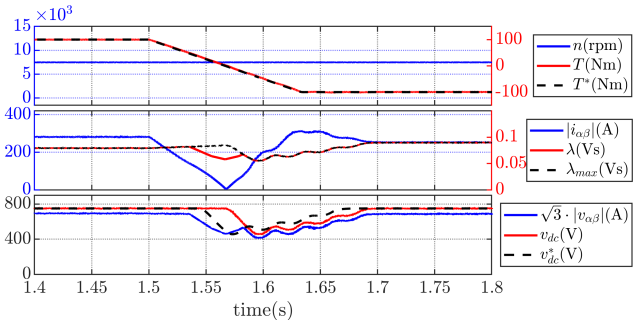

Fig. 11. Torque reversal at 7500 rpm, 100 Nm with a LPF of 30 Hz.

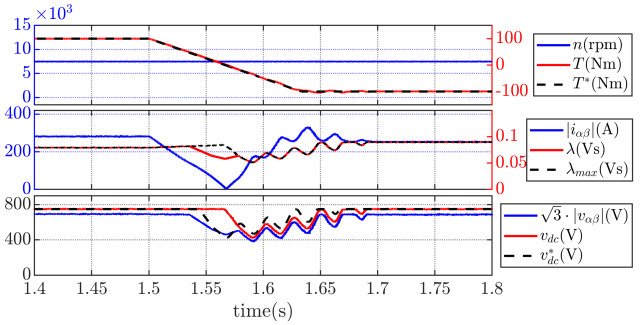

Fig. 12. Torque reversal at 7500 rpm, 100 Nm with a LPF of 150 Hz.

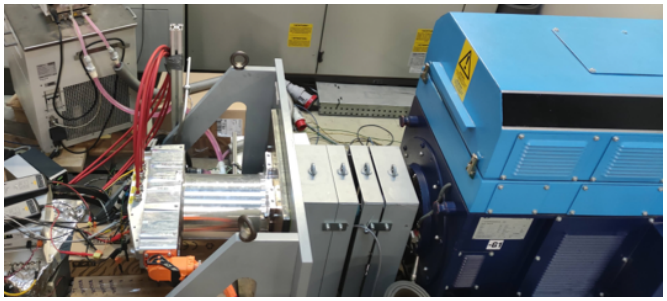

Fig. 13. Test bench for experimental TRL6 validation [6], including the full-scale integrated motor-inverter unit, torque meter and load machine.

in Fig. 1 was tested, with the inverter integrated with the motor, as per the target EV. The rotational speed is imposed by a dyno drive equipped with torque meter, while the motor is torque controlled as per the block diagram in Fig. 3c. According to the final application [6], [7], the drive is tested in 6-phase configuration under CVC-FOC.

Initially, the system stability was tested under severe speed transients, reported in Figs. 14 and 15. Again, the imposed speed slew rate ($\pm$10 krpm/s) is considerably higher than the feasible acceleration on the vehicle. In each Figure, the upper plot depicts the controlled current in the two 3-phase sets, the middle plot reports speed and torque while the lower plot shows the controlled DC-link voltage, together with the minimum v_{dc} required for motor control, i.e., $\sqrt{3}|\boldsymbol{v_{\alpha\beta}}|$. The two Figures report a sharp acceleration from 1 krpm to 10 krpm and deceleration from 10 krpm to 1 krpm, respectively, with a reference torque of 40 Nm. As can be noticed, when the motor operates at 1 krpm, the DC/DC control saturates to the minimum voltage, while at 10 krpm the v^*_{dc} converges to

≈680 V (i.e., lower than the maximum voltage limit of 750 V), which is sufficient for a reliable control of the motor. The DC-link voltage is correctly minimized both at steady state and during transient, while the current and torque controls are practically unaffected, maintaining the reference T^*.

Sharp torque variations are reported in Figs. 16 and 17, depicting a torque rise from zero to 80 Nm (i.e., rated torque) and a torque reversal from 80 Nm to -60 Nm respectively. Also, in this case, the v_{dc} is correctly minimized without affecting the motor control stability, thus reducing the power loss in the converters.

A. WLTP cycle

Finally, a WLTP standard driving cycle was executed both under fixed rated v_{dc}=600 V and with the proposed variable DC-link control. The latter test is reported in Fig. 18. The goal of this test is to evaluate the energy saving obtained with the proposed technique. The reference torque corresponding to the WLTP speed profile was computed based on the donor vehicle characteristics [6]. Under these conditions, v_{dc}^* saturates to the minimum limit for most of the WLTP cycle, while the variable DC-link control becomes effective in the high and very-high speed sections. The control results smooth and stable, the torque control is accurate and the DC-link voltage is correctly minimized over the entire cycle. The power loss in the DC/DC converter, inverter and motor were measured and averaged over the WLTP cycle, as reported in Table II. For the two converters, the table reports the aggregate of conduction and switching losses. As detailed in Section III-A, only the latter ones significantly vary with v_{dc}, so the efficiency improvement obtained with the proposed variable DC-link technique is associated with a reduction in the switching losses of the two converters. As can be seen, the higher benefits are obtained for the DC/DC converter, with a significant loss reduction of 31.7%. A lower advantage is found in the inverter, which can be explained by considering that the inverter adopts SiC power Mosfets with low switching losses, while the conduction losses are predominant and not significantly influenced by v_{dc}. Still, a relevant loss reduction of around 9.5% is obtained. As expected from Section III-B, a limited loss reduction in the machine could also be observed, but this is minor if compared

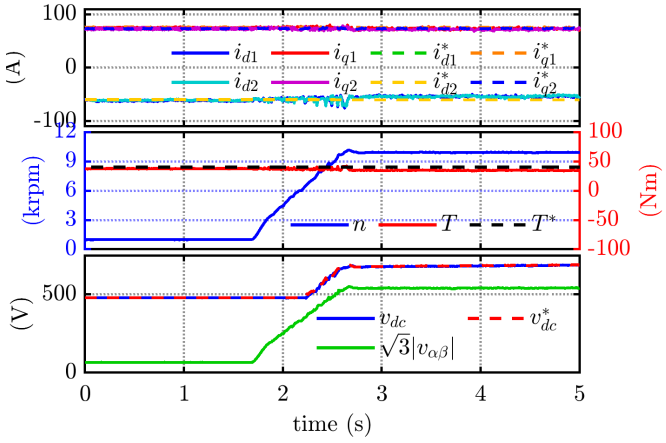

Fig. 14. Experimental: sharp acceleration (10000 rpm/s) from 1 krpm to 10 krpm at 40 Nm load under variable DC-link. From top to bottom: dq currents; motor speed and torque; v_{dc} and voltage amplitude.

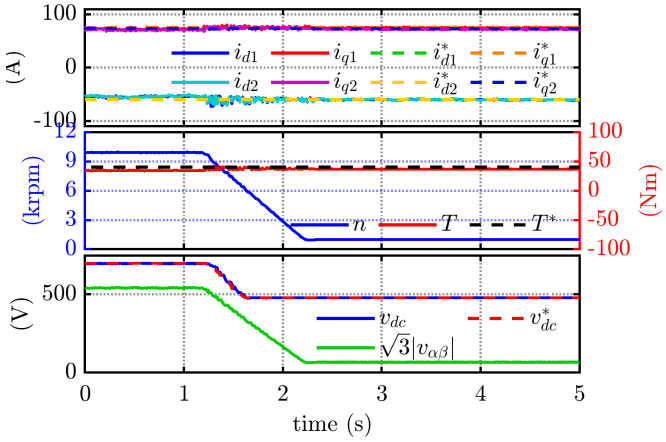

Fig. 15. Experimental: sharp braking (-10000 rpm/s) from 10 krpm to 1 krpm at 40 Nm load under variable DC-link. From top to bottom: dq currents; motor speed and torque; v_{dc} and voltage amplitude.

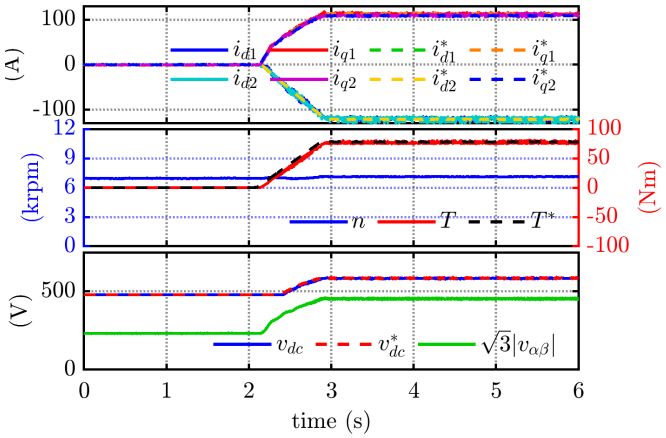

Fig. 16. Experimental: sharp torque variation from 0 Nm to 80 Nm (rated load) at 5 krpm under variable DC-link. From top to bottom: dq currents; motor speed and torque; v_{dc} and voltage amplitude.

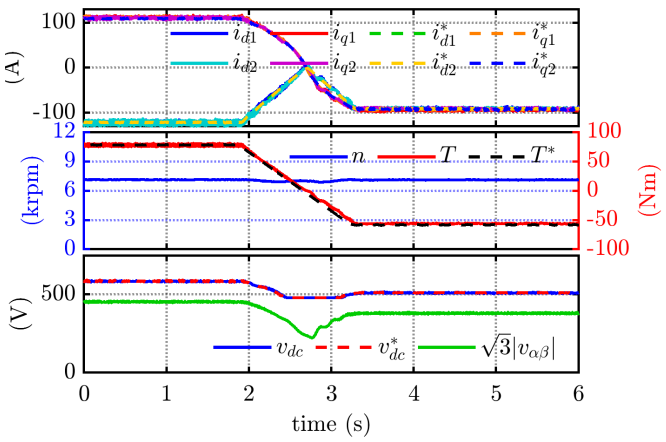

Fig. 17. Experimental: sharp torque reversal from 80 Nm to -60 Nm at 5 krpm under variable DC-link. From top to bottom: dq currents; motor speed and torque; v_{dc} and voltage amplitude.

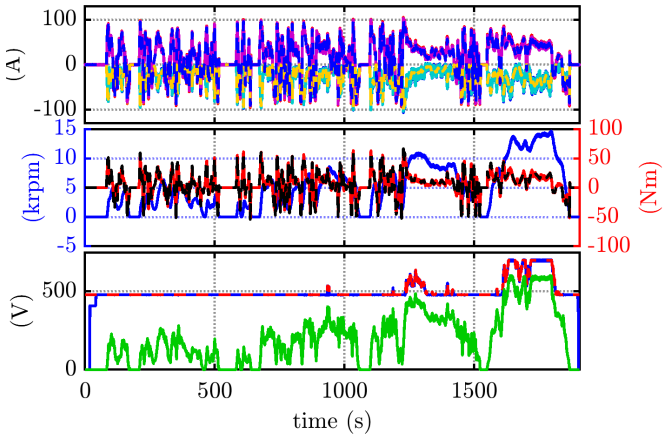

Fig. 18. Experimental: WLTP driving cycle for A-segment BEV under variable DC-link. From top to bottom: dq currents; motor speed and torque; v_{dc} and voltage amplitude.

TABLE II
AVERAGE POWER SAVING UNDER WLTP CYCLE.

	DC/DC loss	Inv. loss	Motor loss	Total loss
Fixed v_{dc}=650 V	511 W	475 W	711 W	1696 W
Variable v_{dc}	349 W	430 W	695 W	1474 W
Loss reduction	31.7%	9.5%	2.2%	13.1%

with the power saving in the converters. Overall, the proposed variable DC-link control permits reducing the losses in the full drivetrain by approximately 13% under WLTP conditions.

IX. CONCLUSIONS

This work proposes a simple and effective strategy for controlling the variable DC-link of an EV equipped with a DC/DC converter. The core of the algorithm is to minimize online the DC-link voltage on varying the drive operating point without affecting the motor control performance, thus permitting MTPA operation up to the maximum possible speed and without limiting the motor control bandwidth. The algorithm is independent of the adopted motor control strategy, it is easily adapted to multi-three-phase applications and can operate even if the inverter and the DC/DC converter are physically separated, despite the significant communication delay between the two. Therefore, the proposed variable DC-link control and the motor control can be developed and tested separately, permitting high flexibility and debugging options. Despite being originally designed for EVs, the present technique can be implemented in a wide number of applications with controllable DC-link. Extensive simulation and experimental testing at TRL6 on a 135 kW full-scale traction e-axle demonstrate the feasibility and advantages of the proposal.

ACKNOWLEDGMENT

The authors are grateful to the European Commission for the support to the present work, performed within the EU H2020 project FITGEN (Grant Agreement 824335).

The research has been conducted with the support of Power Electronics Innovation Center (PEIC) of Politecnico di Torino.

REFERENCES

[1] IEA, *Global Electric Vehicle Outlook 2022*, available: https://www.iea.org/reports/global-ev-outlook-2022 [Accessed Feb. 2022].

[2] R. Leuzzi, P. Cagnetta, S. Ferrari, P. Pescetto, G. Pellegrino and F. Cupertino, "Transient Overload Characteristics of PM-Assisted Synchronous Reluctance Machines, Including Sensorless Control Feasibility," in *IEEE Transactions on Industry Applications*, vol. 55, no. 3, pp. 2637-2648, May-June 2019.

[3] E. Levi, F. Barrero and M. J. Duran, "Multiphase machines and drives - Revisited," in *IEEE Transactions on Industrial Electronics*, vol. 63, no. 1, pp. 429-432, Jan. 2016.

[4] A. Boglietti, I. R. Bojoi, S. Rubino and M. Cossale, "Overload Capability of Multiphase Machines Under Normal and Open-Phase Fault Conditions: A Thermal Analysis Approach," in *IEEE Transactions on Industry Applications*, vol. 56, no. 3, pp. 2560-2569, May-June 2020.

[5] N. Bianchi, E. Fornasiero and S. Bolognani, "Thermal Analysis of a Five-Phase Motor Under Faulty Operations," in *IEEE Transactions on Industry Applications*, vol. 49, no. 4, pp. 1531-1538, July-Aug. 2013.

[6] H2020 EU FITGEN project. Available: https://fitgen-project.eu/ [Accessed Feb. 2023].

[7] M. Martino, P. Pescetto and G. Pellegrino, "Advanced Functionally Integrated E-Axle for A-Segment Electric Vehicles," *2020 AEIT International Conference of Electrical and Electronic Technologies for Automotive (AEIT AUTOMOTIVE)*, Turin, Italy, 2020, pp. 1-6.

[8] A. Salem and M. Narimani, "A Review on Multiphase Drives for Automotive Traction Applications," in *IEEE Transactions on Transportation Electrification*, vol. 5, no. 4, pp. 1329-1348, Dec. 2019.

[9] K. Toshiyuki, H. Na, K. Eritate, N. Takamatsu, M. Okamura and M. Taki, "Bidirectional DC-DC Converter Utilizing New Loss Reduction Techniques for HV/PHV," *2020 IEEE Applied Power Electronics Conference and Exposition (APEC)*, New Orleans, LA, USA, 2020, pp. 3484-3488.

[10] T. Schoenen, M. S. Kunter, M. D. Hennen and R. W. De Doncker, "Advantages of a variable DC-link voltage by using a DC-DC converter in hybrid-electric vehicles," *2010 IEEE Vehicle Power and Propulsion Conference*.

[11] K. Yamazaki and A. Abe, "Loss Investigation of Interior Permanent-Magnet Motors Considering Carrier Harmonics and Magnet Eddy Currents," in *IEEE Transactions on Industry Applications*, vol. 45, no. 2, pp. 659-665, March-april 2009.

[12] L. Chang, T. M. Jahns and R. Blissenbach, "Estimation of PWM-Induced Iron Loss in IPM Machines Incorporating the Impact of Flux Ripple Waveshape and Nonlinear Magnetic Characteristics," in *IEEE Transactions on Industry Applications*, vol. 56, no. 2, pp. 1332-1345, March-April 2020.

[13] J. Lu, A. Mallik, S. Zou and A. Khaligh, "Variable DC-Link Control Loop Design for an Integrated Two-Stage AC/DC Converter," in *IEEE Transactions on Transportation Electrification*, 2018.

[14] C. Yu, J. Tamura and R. D. Lorenz, "Optimum DC Bus Voltage Analysis and Calculation Method for Inverters/Motors With Variable DC Bus Voltage," in IEEE Trans. on Industry Applications, 2013.

[15] A. Amerise, M. Mengoni, L. Zarri, A. Tani, S. Rubino and R. Bojoi, "Open-ended induction motor drive with a floating capacitor bridge at variable DC link voltage," *2017 IEEE Energy Conversion Congress and Exposition (ECCE)*, Cincinnati, OH, USA, 2017, pp. 3591-3597.

[16] L. Liu, G. Götting and J. Xie, "Torque Ripple Reduction Using Variable DC-link Voltage Technique for Permanent Magnet Synchronous Motor in Battery Electric Vehicle," *2020 IEEE 29th International Symposium on Industrial Electronics (ISIE)*, Delft, Netherlands, 2020, pp. 374-379.

[17] L. Liu, G. Goetting and J. Xie, "Loss Minimization Using Variable DC-Link Voltage Technique for Permanent Magnet Synchronous Motor Traction System in Battery Electric Vehicle," *2018 IEEE Vehicle Power and Propulsion Conference (VPPC)*, 2018, pp. 1-5.

[18] C. Pohlandt and M. Geimer, "Variable DC-link voltage powertrain for electrified mobile work machines," *2015 International Conference on Electrical Systems for Aircraft, Railway, Ship Propulsion and Road Vehicles (ESARS)*, Aachen, Germany, 2015, pp. 1-5.

[19] P. Pescetto, A. Sierra-Gonzalez, E. Trancho and G. Pellegrino, "Variable DC-link Control Strategy for Maximum Efficiency of Traction Motor Drives," *2021 IEEE Energy Conversion Congress and Exposition (ECCE)*, Vancouver, BC, Canada, 2021, pp. 4815-4821.

[20] Technology Readiness Level, available at: https://www.nasa.gov/pdf/458490main_TRL_Definitions.pdf [accessed Feb. 2023].

[21] BRUSA Elektronik BDC546, available at https://www.brusa.biz/portfolio/bdc546/. [Accessed Feb. 2023].

[22] P. Pescetto and G. Pellegrino, "Sensorless magnetic model and pm flux identification of synchronous drives at standstill," *2017 IEEE International Symposium on Sensorless Control for Electrical Drives (SLED)*, Catania, Italy, 2017, pp. 79-84.
[23] Mohan, Ned, Tore M. Undeland, and William P. Robbins, "Power Electronics: Converters, Applications and Design.". Third edition. Hoboken, NJ: John Wiley & Sons Inc, 2002.
[24] L. Liu, X. Ba, Y. Guo, G. Lei, X. Sun and J. Zhu, "Improved Iron Loss Prediction Models for Interior PMSMs Considering Coupling Effects of Multiphysics Factors," in *IEEE Transactions on Transportation Electrification*, 2022.
[25] L. Chang, M. Alvi, W. Lee, J. Kim and T. M. Jahns, "Efficiency Optimization of PWM-Induced Power Losses in Traction Drive Systems With IPM Machines Using Wide Bandgap-Based Inverters," in *IEEE Transactions on Industry Applications*, vol. 58, no. 5, pp. 5635-5649, Sept.-Oct. 2022.
[26] A. Sierra-Gonzalez, P. Pescetto, E. Trancho, E. Ibarra, G. Pellegrino, and F. Alvarez-Gonzalez "Control of dual three-phase IPMSM drives with cascaded DC-link capacitors for third generation electric vehicles" *2021 IEEE Energy Conversion Congress and Exposition (ECCE)*, Vancouver, Canada, 2021.
[27] G. Pellegrino, R. I. Bojoi and P. Guglielmi, "Unified Direct-Flux Vector Control for AC Motor Drives," in *IEEE Transactions on Industry Applications*, vol. 47, no. 5, pp. 2093-2102, Sept.-Oct. 2011.
[28] E. Trancho, E. Ibarra, A. Arias, I. Kortabarria, J. Jurgens, L. Marengo, and A. Fricasse, "PM-assisted synchronous reluctance machine flux weakening control for EV and HEV applications," *IEEE Transactions on Industrial Electronics*, vol. 65, no. 4, pp. 2986–2995, 2018.

Paolo Pescetto , (S'16 – M'19) received the B.Sc. and M.Sc. degrees with full grade and honors from Politecnico di Torino, Turin, Italy, in 2013 and 2015. Since 2015 he worked in the same institution toward the PhD degree obtained "Cum Laudem" in 2019. Since fall 2019 he is working as researcher and tenure track lecturer in the Energy Department of Politecnico di Torino. He is a member of the Power Electronics Innovation Center (PEIC) of Politecnico di Torino. In 2014 he was an Erasmus Student at the Norwegian University of Science and Technology, Trondheim. He authored or co-authored 10+ IEEE journal papers. His main research interests include synchronous motor drives, sensorless control, self-commissioning techniques and integrated battery chargers for EVs. Dr. Pescetto received five IEEE Paper Awards and two IEEE PhD thesis award.

Andres Sierra-Gonzalez received his bachelor and master degree in electronic and electrical engineering in 2008 and 2015 from Andes University, Bogotá, Colombia, and a second M.Eng. degree and a Ph.D. in electronics and telecommunication from the University of the Basque Country, Bilbao, Spain, in 2017 and 2023. From 2009 to 2013, he was an Electronics Engineer in the mining and energy industry. He was a Research Assistant at Andes University, Bogotá, Colombia, from 2014 to 2016. Since 2018, he is Control Systems Researcher applied to electromobility with Tecnalia Research and Innovation, Derio, Spain. He was co-recipient of the Best Paper Award for the IEEE VPPC in 2017.

Fernando Alvarez-Gonzalez received the B.Eng. degree in electronic engineering and M.Eng. degree in electrical and electronic engineering from the University of Oviedo, Asturias, Spain, in 2012 and 2014, respectively. He received the Ph.D. degree in electronic and electrical engineering from The University of Sheffield, Sheffield, U.K., in 2019. From 2018 to 2020 he was a Postdoctoral Research Associate at The University of Sheffield's EMD group. From 2020 he has been a researcher with Tecnalia Research & Innovation. His research interests include modeling, control, fault detection, and condition monitoring of electric machines and power electronics.

Hansjörg Kapeller received the Dipl.-Ing. degree in electrical engineering from Vienna University of Technology, Vienna, Austria, in 2004. Since then he has been a Research Engineer in the field of electric drives at AIT Austrian Institute of Technology, Vienna. His field of work includes the modelling, simulation and control of electric drives including HVAC systems as well as the coordination of international and national research projects. He is also managing AIT's commercial simulation libraries developed at the Competence Unit Electric Vehicle Technologies

Elena Trancho received the M.Sc. degree in automatic and electronic engineering from the University of Deusto, Bilbao, Spain, in 2011, the M.SC degree in electrical engineering from the Institut Nationale Politechnique, Toulouse, France, in 2012, and the Ph.D. degree in automatic and electronic engineering from the University of the Basque Country, Bilbao, Spain, in 2018. From 2012 to 2014, she was an Advanced Flight Control Researcher with Akka Technologies, Toulouse, France. Since 2014, she is an Advanced Drives Control Researcher with Tecnalia Research and Innovation, Basque Country. Her research interests include electric and hybrid vehicles, variable-speed drives, advanced control strategies, and sensorless techniques.

Gianmario Pellegrino (F' 22, SM '13, M'06) is Professor of Power Converters, Electrical Machines and Drives at Politecnico di Torino, Turin, Italy. He was a visiting fellow at Aalborg University, the University of Nottingham, and the University of Wisconsin-Madison. Dr. Pellegrino is author of the open-source platform SyR-e for the design of electrical motors and drives, constantly developed and validated in the context of collaborations with the industry, and widely adopted world-wide. Dr. Pellegrino is an IEEE Fellow, an Associate Editor for the IEEE Transactions on Industry Applications and the recipient of the 8th Grand Nagamori Award. The research impact is summarized by 60+ IEEE journal papers, eight patents and nine Best Paper Awards. He is currently a member of the Power Electronics Interdepartmental Center (PEIC) of Politecnico di Torino, a member of the Advisory Board of PCIM Europe, and the Rector's Advisor for Interdepartmental Centres of Politecnico di Torino